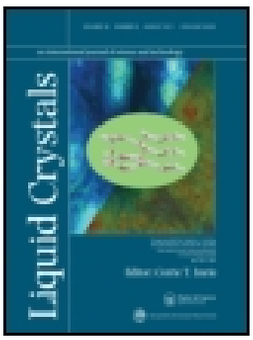

Liquid Crystals

ISSN: 0267-8292 (Print) 1366-5855 (Online) Journal homepage: http://www.tandfonline.com/loi/tlct20

Influence of polar dopant on internal configuration of azoxybenzene nematic-in-water droplets

A. V. Dubtsov , S. V. Pasechnik , D. V. Shmeliova , D. A. Semerenko , Aleš Iglič & Samo Kralj

To cite this article: A. V. Dubtsov , S. V. Pasechnik , D. V. Shmeliova , D. A. Semerenko , Aleš Iglič & Samo Kralj (2017): Influence of polar dopant on internal configuration of azoxybenzene nematic-in-water droplets, Liquid Crystals, DOI: 10.1080/02678292.2017.1336676

To link to this article: http://dx.doi.org/10.1080/02678292.2017.1336676

Published online: 11 Jun 2017.

LIQUID CRYSTALS, 2017
https://doi.org/10.1080/02678292.2017.1336676

Taylor & Francis
Taylor & Francis Group

ARTICLE

Influence of polar dopant on internal configuration of azoxybenzene nematic-in-water droplets

A. V. Dubtsov [a], S. V. Pasechnik [a], D. V. Shmeliova [a], D. A. Semerenko [a], Aleš Iglič [b] and Samo Kralj [c,d]

[a]Problem Laboratory of Molecular Acoustics, Moscow Technological University, Moscow, Russia; [b]Faculty of Electrical Engineering, University of Ljubljana, Ljubljana, Slovenia; [c]Condensed Matter Physics Department, Jožef Stefan Institute, Ljubljana, Slovenia; [d]Faculty of Natural Sciences and Mathematics, University of Maribor, Maribor, Slovenia

ABSTRACT

We report the study of optical textures and director configurations within nematic-in-water microdroplets of the liquid-crystalline mixtures based on azoxybenzene and cyanobiphenyl (as a polar dopant). Both pure azoxybenzene and polar dopant materials exhibited bipolar configuration within liquid-crystalline droplets, whereas their mixtures at appropriate concentrations spontaneously formed radial droplets. It was found that increasing of the dopant's concentration resulted in the forward tangential-homeotropic and reentrant homeotropic-tangential anchoring transitions. We also triggered bipolar-to-radial structural transition by UV irradiation providing trans-cis isomerisation of nematogens. Critical irradiation time needed for radial configuration formation was found to decrease with concentration of polar dopant. Mesoscoping modelling is proposed to explain main experimental results. The presented data are discussed for chemical and biological sensing applications.

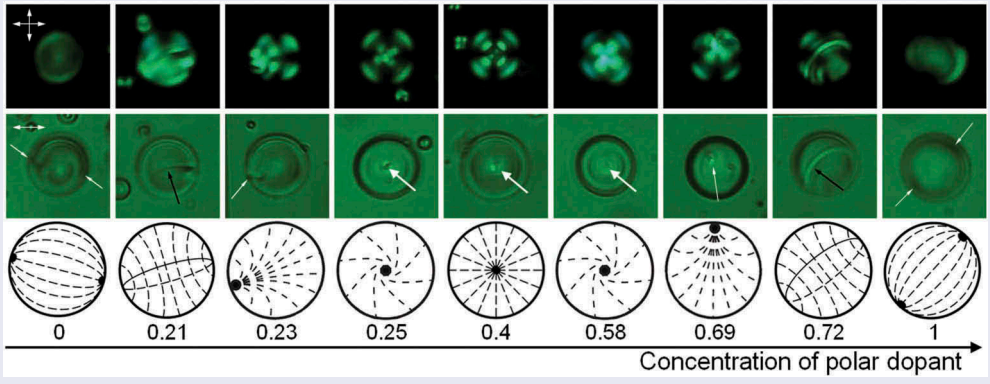

ARTICLE HISTORY
Received 28 February 2017
Accepted 27 May 2017

KEYWORDS
Liquid crystals; azoxybenzene; polar dopant; microdroplets; director configuration; UV irradiation; trans-cis isomerisation; structural transformation

1. Introduction

Liquid crystals (LCs) play an outstanding role in modern display industry. Operation of a majority of liquid crystal displays (LCDs) is based on electro-optical effects imposed by an external electric-field-driven changes in LC orientational ordering and in related optical properties. Such changes are enabled by a relatively weak power consumption and low operating voltages, providing principal advantages of LCDs with respect to competing materials. Extreme response of LCs is due to existence of Goldstone modes in nematic director field, yielding soft character. In general, softness also provides LCs with relatively high sensitivity to the action of other perturbations, like thermal fields, light irradiation or low-frequency mechanical perturbations [1]. Consequently, LCs represent promising material to be exploited in various sensor applications. Of particular interest are LC-based sensor aimed to detect biological nano-objects (lipids, viruses and bacteria). Pioneering investigations [2] were performed in planar geometries of nematic LCs in contact with a water suspension of biological objects. Changes in the surface orientation of LC layer induced by bio-objects were exploited as the key detection mechanism. These changes were detected using polarised microscopy providing information on presence and concentration of biological objects. Furthermore [3], it was found that LC droplets immersed in a suspension of bio-objects changed their LC orientational structure for significantly lower concentrations in comparison to planar LC geometries. This geometry-enhanced

CONTACT A. V. Dubtsov alexanderdubtsov@gmail.com

concentration sensitivity could be readily exploited in various biomedical applications. To reach this goal, it is necessary to identify and clarify key physical mechanisms involved. In particular, it is of interest to explore impacts of the size of LC droplets, ionic strength, temperature, etc., on structural transitions in LC droplets induced by biological objects. Several studies have already been carried out in LC droplet immersed in isotropic media [4,5]. Basic interest to such systems was due to possible influence of the boundary's curvature and strong confinement on the LC orientational structure and thermodynamic behaviour [5]. Such investigations had been also stimulated by the perspectives of possible usage of composite LC materials in the display, photonic and, more recently, sensor applications. In particular, various thermodynamically stable LC structures were determined on varying LC elastic properties, droplet radius and surface anchoring strength [5,6]. External perturbations of a different nature may lead to structural transformations within the droplets. Such changes can be caused by electric [7,8] (magnetic [9–11]) fields and temperature gradient [12,13], hydro-dynamic flows [14]. For advanced sensor technology is of particular interest the application of orientational transitions within LC droplets triggered by chemical and biological impurities (see recent reviews [15,16]). In particular, the endotoxins [17], lipids [2,18], viruses [19], bacteria [19], organophosphates [20], proteins [21] and glucose [22] can localise at the LC–water interface and cause planar-homeotropic anchoring (or vice versa) transition within LC droplets. Moreover, topological defects in LCs can be considered as platform for self-assembly of biological impurities [23–25].

Recently [26], it was found that structural transitions could be caused by UV irradiation of photosensitive LC droplets dispersed in water. In this case, the initial bipolar configuration was transformed into the radial one at a critical irradiation time t_c, which was equal to several minutes. The critical irradiation time increased with the droplet's size and decreased with the light intensity. It was also shown that t_c could be effectively decreased by adding into water the biological nanoparticles (phospholipids) of rather low concentrations. Such effects were explained by similar action of nanoparticles and UV-induced *cis*-isomers, localised at LC–water interface on the configuration of LC within the droplets. For high enough concentration of *cis*-isomers, homeotropic anchoring conditions were established at the interface due to dipole–dipole and steric interactions. This proof-of-principle suggested that UV irradiation could be exploited as a new type of LC biosensor, based on measurements of t_c needed to trigger a bipolar–radial structural transition. It was established that UV-induced bipolar-to-radial transition took place for the nematic mixture of azoxybenzene compounds (ZhK-440) with some amount of polar dopant whereas such transition was not observed in the absence of the dopant.

In this article, we present the results of experimental and theoretical study of the influence of polar dopant (cianobiphenyl) added to the nematic mixture (ZhK-440) on optical textures and director configurations, formed within LC droplets under the action of water environment and UV irradiation. We also consider possible physical mechanisms responsible for observed phenomena. The plan of the article is as follows. In Section 2, we describe our experimental set-up. In Section 3, we present our theoretical analysis. In Section 4, we present and discuss our measurements. In Section 5, we make conclusions.

2. Experimental

Our primary LC material ZhK-440 (NIOPIK production) is a mixture of two-thirds p-n-butyl-p-methoxyazoxybenzene and one-third p-n-butyl-p-heptanoylazoxybenzene. It possesses a nematic phase from 0 to 75°C [27] if LC molecules exhibit *trans*-isomer configuration. ZhK-440 was doped with 4′-pentyl-4-cyanobiphenyl (5CB, Alfa Aesar). Different weight concentrations c were used, ranging from 0 to 1. Here $c = 0$ ($c = 1$) corresponds to pure ZhK-440 (5CB) material. Deionised water of resistivity 18.2 MΩcm was used as dispersed medium. The emulsions with micrometer-sized LC droplets were formed by sequential sonication and vortexing of 2 μl of mixture ZhK-440/5CB in 2 ml of water. Several processes of sonication and vortex mixing allow obtaining droplets with diameter ranging from 1 to 12 μm. The LC emulsions were dispensed onto glass microscope slide by micro pipette for optical texture observations and light irradiation. Orientational structures of LC within the droplets were determined by observation under POLAM L-213M (LOMO) transmitted light microscope connected with a digital camera. Halogen lamp of the microscope was used to induce *trans-cis* isomerisation of ZhK-440 molecules enabling us to trigger structural transitions within LC droplets. Linearly polarised light irradiated bottom side of the microscope glass plate with deposited LC emulsion. The emulsions were irradiated with relatively wide spectrum (including both 365- and 450-nm wavelengths playing important role in the *trans-cis* isomerisation) [28]. Intensity of linearly polarised light was controlled at $\lambda = 365$ nm and varied from $I = 4$to 40 mW/m^2. To prevent negative light irradiation, we used green filter with a peak at $\lambda = 530$ nm. We observed and characterised the LC droplets with diameter ranged from 1 to 12 μm using immersion objective with 100× magnification. Translating and rotating droplets were analysed to

prevent observation of droplets interacting with surface of microscope glass plate. Optical textures of LC droplets were analysed in crossed polarisers at different angles of microscope table and also in bright field in polarised light without analyser. Full wave plate placed between the sample and analyser was used for determination of internal director configuration within the droplets. The size distributions of the LC emulsion droplets were determined from optical micrographs using PC software. Multiple images of each droplet were taken to determine the time-dependent optical textures of the droplet. The observations were made at room temperature $T \sim 24^{\circ}$C.

3. Theoretical modelling

In this section, we make theoretical analysis of key phenomena which are expected to play dominant or important role in our experimental measurements. We first consider interaction of LC molecules carrying electrical dipoles with a dielectric interface. We show that dipole interactions favour homeotropic anchoring. Then we analyse impact of assembling of electric dipoles on their resulting effective electric field. We demonstrate that the electric field displays relative strong changes on increasing the assembly from nanometre to larger scales. A study of the impact of an external electric field on relative permittivity of water follows. Finally, we estimate critical UV irradiation time to trigger a structural transition in spherical LC droplets via photo-isomerisation of LC molecules.

3.1. Adsorption strength of LC-isomers at the water–LC interface

We consider a LC molecule isomer possessing the electric dipole

$$\vec{p} = p^{(iso)}(\vec{e}_x \sin\theta + \vec{e}_y \cos\theta) \tag{1}$$

placed at $(x = 0, y = -h/2)$ below a straight water–LC interface located at $y = 0$. Therefore, LC medium is placed in the region $y < 0$. The unit vectors $\{\vec{e}_x, \vec{e}_y\}$ define the two-dimensional Cartesian coordinate frame, and the interface normal points along $\vec{e}_y$. The isomer's dipole strength is labelled by $p^{(iso)}$. In a rough estimate, we assign the spatially homogeneous dielectric constant ε to the water medium. In the dielectric, the image dipole [29]

$$\vec{p}' = p^{(iso)}(\varepsilon - 1)/(\varepsilon + 1)(-\vec{e}_x \sin\theta + \vec{e}_y \cos\theta) \tag{2}$$

appears at $(x = 0, y = h/2)$. The electrostatic interaction between the dipole and its image dipole reads

$$W^{(iso)} = -\frac{p^{(iso)2}}{4\pi\varepsilon_0 h^3}\left(\frac{\varepsilon - 1}{\varepsilon + 1}\right)(1 + \cos^2\theta). \tag{3}$$

For LC of our interest, it holds $p^{(cis)} \sim 5p^{(trans)}$ [29], where $p^{(cis)}$ ($p^{(trans)}$) marks the magnitude of the *cis*-isomer (*trans*-isomer). Recent analyses suggest that these electrostatic interactions are overwhelmed by steric interactions. These enforce homeotropic anchoring (i.e. $\theta = 0$) if *cis*-isomers are prevailing at the LC–dielectric interface. On the other hand, *trans*-isomers enforce tangential anchoring ($\theta = \pi/2$). The ratio of corresponding electrostatic interactions is roughly equal to $W^{(cis)}/W^{(trans)} = 2p^{(cis)2}/p^{(trans)2} \sim 50$ assuming that value of h is comparable in both cases. Therefore, *cis*-isomers are significantly stronger electrostatically coupled at the LC–dielectric interface.

3.2. Electric field produced by different assemblies of electric dipoles

We next demonstrate that different assemblies of electric dipoles yield markedly quantitatively different electric field spatial profiles. To demonstrate this, we consider a simplest possible case resembling situations encountered in our experiments. For this purpose, we consider a cylindrically symmetric spatially homogeneous assembly of electric dipoles of surface density σ and employ the cylindrical coordinates (x,z) (see Figure 1). We assume that the dipoles are aligned along the z-axis. In the following, we calculate the resulting electric field along the symmetry axis as a function of the cylinder radius ρ. Therefore, relatively small (large) values of ρ mimic nanoparticle-like (semi-macroscopic) objects.

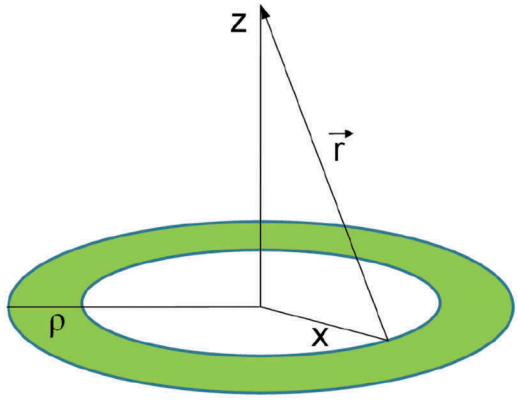

Figure 1. (Colour online) Effective dipole on the surface of a disc-like assembly of unit dipoles.

The magnitude of the total electric dipole moment dp of a narrow ring of dipoles at distance x is given by $\mathrm{d}p = \sigma 2\pi x \mathrm{d}x$. The resulting electric potential $\mathrm{d}U$ is expressed as [30]

$$\mathrm{d}U = \frac{\mathrm{d}\vec{p}\cdot\vec{r}}{4\pi\varepsilon_0 r^3} = \frac{\sigma z x \mathrm{d}x}{2\varepsilon_0 (x^2+z^2)^{3/2}}, \tag{4}$$

where $r = \sqrt{x^2+z^2}$ (see Figure 1). The integration over the whole cylinder yields

$$U = \frac{\sigma}{2\varepsilon_0}\left(1 - \frac{1}{\sqrt{1+(\rho/z)^2}}\right), \tag{5}$$

The corresponding electric field $E = -\partial U/\partial z$ can be expressed as

$$E = E_0 \frac{\rho_0}{\rho}\left(1+\frac{z^2}{\rho^2}\right)^{-3/2}, \quad \text{where } E_0 = \sigma/(2\varepsilon_0\rho_0). \tag{6}$$

3.3. Relative permittivity of water in external electric field

In the following, we derive the dependence of relative water permittivity (ε_w) on the magnitude of electric field. In the model, the electronic polarisation of water molecules is taken into account by assuming that the point-like rigid (permanent) dipole with dipole moment amplitude p is embedded in the centre of a sphere [31,32], and with the volume approximately equal to the average volume of a water molecule (Figure 2). The permittivity of the sphere is n^2, where n is the optical refractive index of water [31].

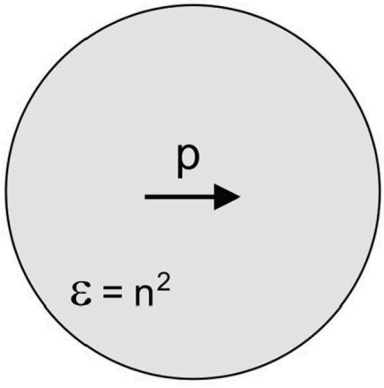

Figure 2. A single water molecule is described as a sphere with permittivity $\varepsilon = n^2$, where $n = 1.33$ is the optical refractive index of water. The point-like rigid (permanent) dipole with the magnitude p located at the centre of the sphere [31,32].

The external water dipole moment with the magnitude p_0 of a point-like dipole at the centre of the sphere with permittivity $\varepsilon = n^2$ can then be expressed in the form [33] $p_0 = 3p/(2+n^2)$ which yields

$$p = \left(\frac{2+n^2}{3}\right)p_0. \tag{7}$$

Neglecting the short-range interactions between dipoles, the local electric field strength at the centre of the sphere at the location of the permanent (rigid) point-like dipole (Figure 2) equals to [33]

$$E_\mathrm{c} = \left(\frac{3\varepsilon_\mathrm{w}}{2\varepsilon_\mathrm{w}+n^2}\right)E. \tag{8}$$

Since $\varepsilon_\mathrm{w} \gg n^2$ (for small enough E) it follows from Equation 8:

$$E_\mathrm{c} = \frac{3}{2}E. \tag{9}$$

Taking into account Equations 7 and 9 the energy of the point-like dipole p in the local field E_c at the centre of the sphere (see Figure 2) is then

$$W_d = -\vec{p}\cdot\vec{E}_c = pE_c\cos\omega = \gamma p_0 E\cos\omega, \tag{10}$$

where ω describes the orientation of the dipole moment vector with respect to vector $-\vec{E}_c$ and γ is [31,32]:

$$\gamma = \frac{3}{2}\left(\frac{2+n^2}{3}\right). \tag{11}$$

The probability of finding a water dipole vector in an element of a solid angle $\mathrm{d}\Omega = 2\pi\sin\omega\mathrm{d}\omega$ is proportional to the Boltzmann factor $\exp(-W_d\beta)$, where $\beta = 1/kT$, therefore

$$\langle\cos\omega\rangle = \frac{\int_0^\pi \cos\omega e^{-\gamma p_0 E\beta\cos\omega}\sin\omega\mathrm{d}\omega}{\int_0^\pi e^{-\gamma p_0 E\beta\cos\omega}\sin\omega\mathrm{d}\omega} = -L(\gamma p_0 E\beta), \tag{12}$$

where $L(u) = \coth(u) - 1/u$ is the Langevin function. By taking into account Equations 7 and 12, the magnitude of polarisation vector of water molecules $\vec{P}$ due to the net orientation of water dipoles can be then expressed as [31,32]

$$P = n_w p\langle\cos\omega\rangle = -n_w p_0\left(\frac{2+n^2}{3}\right)\langle\cos\omega\rangle = -n_w p_0\left(\frac{2+n^2}{3}\right)L(\gamma p_0 E\beta), \tag{13}$$

where n_w is the number density of water dipoles, p_0 is the magnitude of the water external dipole moment and ω is the angle between the gradient of electric potential and dipole moment vector. The relative water permittivity ε_w as a function of the magnitude of electric field strength E can then be written as

$$\varepsilon_w = n^2 + \frac{|P|}{\varepsilon_0 E} = n^2 + \frac{n_w p_0}{\varepsilon_0}\left(\frac{2+n^2}{3}\right)\frac{L(\gamma p_0 E\beta)}{E}, \quad (14)$$

where ε_0 is permittivity of the free space. In the limit of vanishing electric field strength $(E \to 0)$, the above expression for relative permittivity of water gives the Onsager limit

$$\varepsilon_w = n^2 + \left(\frac{2+n^2}{3}\right)^2 \frac{n_w p_0^2 \beta}{2\varepsilon_0}. \quad (15)$$

For $p_0 = 3.1D$ and $n_w/N_A = 55$ mol/l [31,32], Equation 15 yields the value $\varepsilon_w = 78.5$ at room temperature, where N_A is Avogadro number.

3.4. The critical irradiation time

We consider a nematic LC exhibiting UV irradiation-driven *trans-cis* isomerisation. In the following, we present a simple model describing the UV-driven *bipolar–radial* structural transition in a nematic droplet. Based on it, we derive an estimate for the critical irradiation time t_c as a function of droplet radius R and UV irradiation intensity I. In our previous paper [26], we showed that the *bipolar–radial* transition is enabled by assembling of *cis*-isomers at the LC–water interface. When the ratio

$$\mu = N_c^{(i)}/N_t^{(i)} \quad (16)$$

reaches its critical value μ_c the structural transition takes place. Here, $N_c^{(i)}$ and $N_t^{(i)}$ determine the number of *cis*-isomers and *trans*-isomers at the droplet interface, and the superscript (i) stands for the interface. We further denote with N_t (N_c) the total number of *trans*-isomers (*cis*-isomers) within the droplet and the total number of LC molecules is equal to $N = N_t + N_c$. We set that the UV irradiation is switched on at the time $t = 0$. In the initial state, all LC molecules are in *trans*-state, promoting tangential anchoring condition. Within an infinitesimally small time interval dt, the number of generated *cis*-isomers is roughly given by

$$\mathrm{d}N_c = -\mathrm{d}N_t = N_t^{(irr)} I\sigma \mathrm{d}t, \quad (17)$$

where σ is a material property and $N_t^{(irr)}$ represents number of UV-irradiated *trans*-isomers. In our experiments, LC samples are irradiated from a single direction. We assume that the UV absorption is efficient only in a narrow frontal lobe within the penetration thickness ξ_p. It roughly holds

$$N_t^{(irr)} \sim N_t \xi_p / R. \quad (18)$$

The integration of Equation 17 yields

$$N_t = N - N_c = N(1 - e^{-t/\tau}), \quad (19)$$

where

$$\tau = R/(\xi_p \sigma I). \quad (20)$$

We assume that the locally generated *cis*-isomers are 'immediately' uniformly redistributed over the whole volume. Namely, the characteristic diffusion time τ_{LC} when a LC molecule propagates for a distance R is relatively small with respect to t_c. We estimate it using expression for isotropic random walk-type diffusion of spherical objects, i.e.

$$\tau_{LC} \sim \frac{R^2}{4D}, \quad (21)$$

where $D \sim 6 \times 10^{-6}$ cm^2/s is average diffusion constant of LC molecules. For $R = 1$ μm one gets $\tau_{LC} \sim 0.4$ ms. Note further that LC droplets also rotate in the solution. Their typical rotation time is approximated by the Einstein expression

$$\tau_r = \frac{\eta v}{k_B T}, \quad (22)$$

where $\eta \sim 10^{-3}$ Pa · s is the viscosity of water, k_B is the Boltzmann constant and $v \sim \frac{4\pi R^3}{3}$ stands for the volume of a LC droplet. For $R = 1$ μm and $T = 300$ K it follows $\tau_r \sim 1$ s. Therefore, during t_c we can assume that all LC droplets surface areas are evenly exposed to UV irradiation. With this in mind, we get an estimate for the volume concentration $n_c \sim N_c/(4\pi R^3/3)$ of *cis*-isomers

$$n_c \sim \frac{1 - e^{-t/\tau}}{v}. \quad (23)$$

Here $v \sim ad$ estimates volume of a roughly cylindrically shaped LC molecule, a estimates its surface area and d its length. Note that we set that main geometric characteristics of *cis* and *trans*-isomers are equal. Taking into account the interface area conservation condition $N4\pi R^2 \sim a(N_c^{(i)} + N_t^{(i)})$ we get

$$N_c^{(i)} \sim \frac{4\pi R^2 d}{v}(1 - e^{-t/\tau}). \quad (24)$$

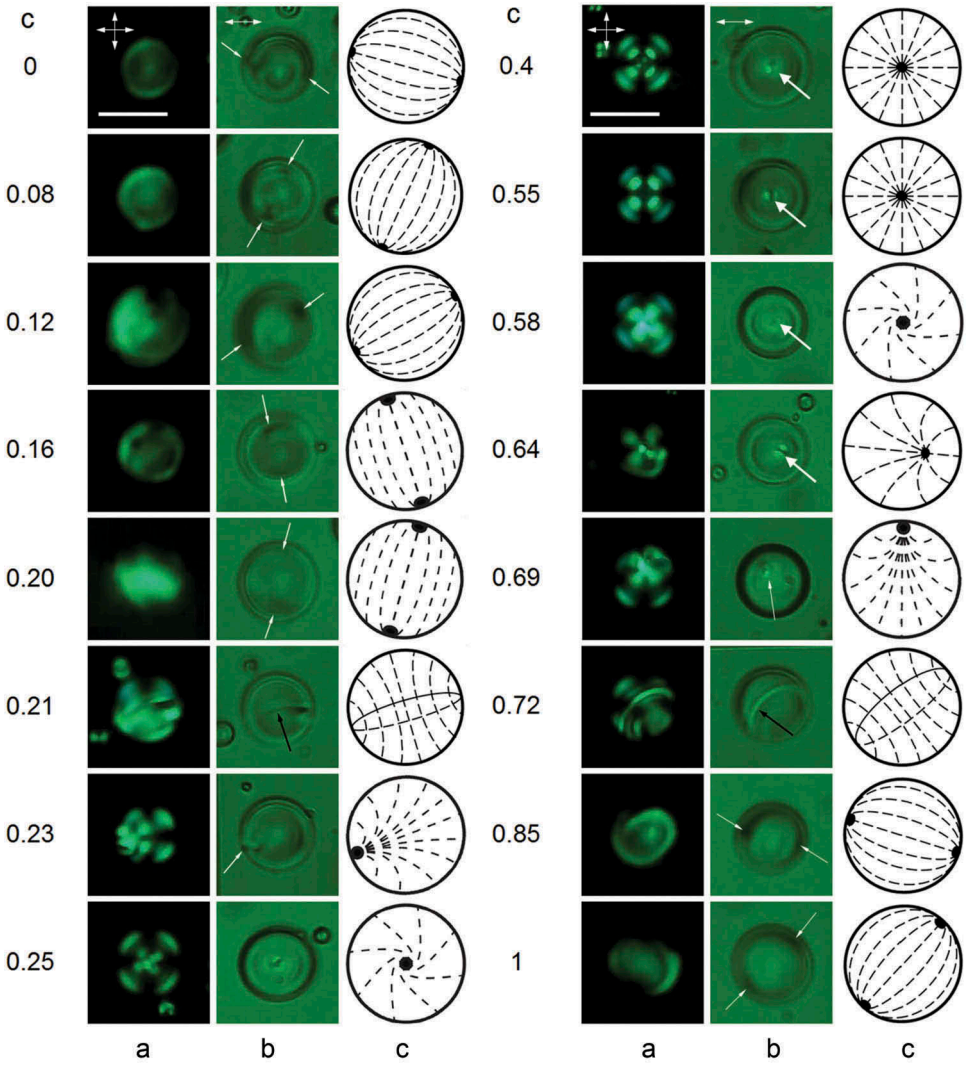

Figure 3. (Colour online) Optical textures (A, B) of LC droplets at variation of 5CB concentration c in the mixture ZhK-440/5CB. Double-headed arrows indicate the orientation of the crossed polarisers (A) and the single polariser (B). Single-headed arrows indicate positions of topological defects (boojum, small white arrow; hedgehog, large white arrow; and disclination ring, black arrow). (C) Schematic sketches of characteristic nematic director profiles corresponding to the optical textures. Scale bar is 10 μm.

Considering Equations 19 and 24, we obtain

$$t_c \sim \frac{R}{I\sigma\xi_p^c}\ln(1+\mu_c), \tag{25}$$

Note that μ_c is also weakly R-dependent(see [26]).

4. Results

We analyse nematic structures in spherical LC droplets of radia R dispersed in water where structures are probed by means of polarising microscopy. Either bipolar-type or radial-type structures are observed, which we henceforth label as *bipolar* and *radial* structures, respectively. Their typical nematic director profiles are schematically depicted in panel C of Figure 3.

Of our particular interest is the impact of nematogenic dopants in homogeneous LC mixtures on the critical irradiation time t_c needed to trigger the *bipolar–radial* structural transition. For this purpose, we study binary mixtures A + B. Here A stands for the photosensitive azoxybenzene LC ZhK-440, exhibiting *trans-cis* conformational change under the UV irradiation. The non-photosensitive dopant component B is represented either by a polar 4-n-pentyl-4′-cyanobiphenyl (5CB) or a nematic mixture E7 or nonpolar p-n-methoxybenzylidene-p'-butylaniline (MBBA) nematogen. Essential material properties of main LCs used in

Table 1. Elastic and dielectric parameters of main LCs used in our study deep in their nematic phase.

	ZhK-440 [27]	5CB [34]	E7 [35]	MBBA [36]
$\Delta\varepsilon$	−0.4	11.5	14	−0.7
K_{11} (10^{-12} N)	8.5	6.4	10.8	5.8
K_{22} (10^{-12} N)	7.2	3	7.4	3.4
K_{33} (10^{-12} N)	10.3	10	17.5	7

our study are assembled in Table 1. Our prime interest is to investigate the role of polar character of B on t_c.

Note that chosen isolated B components in their nematic phase promote tangential anchoring at B-water interfaces. In the following we demonstrate impacts of (i) the polar character of the component B and its concentration c, (ii) UV irradiation intensity I and (iii) droplet radius R on t_c deep in the nematic phase of homogeneous mixtures. Of particular interest is to find regimes where the *bipolar–radial* transition could be realised with critical irradiation times below 1 min which is of interest for several potential applications.

4.1. Influence of c in the absence of UV light irradiation

In our first set of experiments, we investigated the influence of 5CB concentration c on the nematic director field configuration of LC droplets in absence of UV light irradiation.

Figure 3 shows optical textures and the corresponding nematic director configurations of micrometer-sized droplets on increasing c. We probed 5CB concentrations c = (0,0.08,0.12,0.16,0.20,0.21,0.23,0.25,0.40,0.55,0.58, 0.64,0.69,0.72,0.85,1), where $c = 1$ corresponds to the pure 5CB material.

For pure ZhK-440 ($c = 0$), we observed droplets with diameter larger than 2 μm to exhibit *bipolar* configuration. For example, Figures 3(a,b) show crossed polarised light and bright field micrographs, respectively, of a *bipolar* droplet with diameter 10.5 ± 0.5 μm. A bipolar configuration is characterised by LC molecules oriented tangentially at LC–water interface and two surface point defects (boojums) at the opposite poles of the droplet. Bright field in the droplet was also observed when its optical axis rotated at 45°, respectively, to the crossed polarisers. Similar optical textures were observed for concentration window $c = 0 \ldots 0.2$ but the black points at the opposite poles of the droplets loose their darkness with concentration c and completely vanished for $c = 0.21$. Such behaviour reflects more uniform director distribution within the droplets. For concentration $c = 0.21$, we observed bright (dark without analyser) loop close to the droplet equator which changed direction at rotation of the droplet, respectively, to the crossed polarisers. In this case, configuration is an axial with a line defect where director is characterised by perpendicular or tilted orientation at the surface. We found no declination loop for concentration $c = 0.23$. Instead, we observed polarised micrographs with crossed extinction bands with strong distortion outside centre of the droplet and point defect near the surface in bright field. The various positions of the point defect located on the surface droplet under Brownian motion confirmed preradial director configuration. At $c = 0.25$, we found twisted extinction bands in crossed polarisers with invariant point defect in the centre of the droplet in the bright field, which refers to the twist radial configuration. Figure 4 shows optical textures of ZhK 440/5CB droplets with concentration $c = 0.25$ at different droplet radius R.

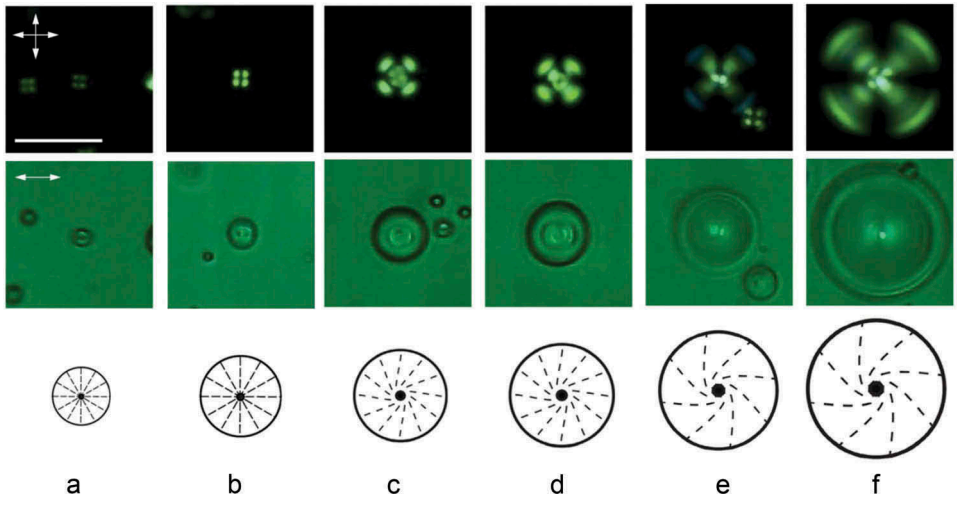

Figure 4. (Colour online) Optical textures in crossed polarisers (top panel) and bright field (medium panel) of LC droplets at various droplet radius at fixed 5CB concentration $c = 0.25$ in the mixture ZhK-440/5CB. Schematic sketches (lower panel) of characteristic nematic director profiles corresponding to the optical textures. Scale bar is 10 μm.

As shown in Figure 4 twist structure changed to common radial configuration (characterised by interference image with uniform invariant cross like extinction bands) with decreasing of the droplet radius (Figure 4). A radial-type configuration was also observed for $c = 0.4$ at different droplet diameters that ranged from 1 to 10 μm. Further increasing of c from 0.55 to 1 resulted in reverse radial-bipolar structural transformation. Several previous reports had also showed formation of tangential anchoring with bipolar configuration in droplets for pure nematic 5CB at water interface [3,17,37].

To summarise, on increasing c, we find three different regimes in absence of UV irradiation as it is evidently shown in Figure 3. As shown in Figure 3, we plot typical interference patterns for fixed radius R revealing characteristic nematic textures in these regimes. For $c \leq 0.2$ and $c \geq 0.85$, the LC droplets exhibit *bipolar* structures. Within the concentration window $0.25 \leq c \leq 0.58$, the droplets spontaneously form *radial* structures. Intermediate structures with homeotropic anchoring are formed for $0.2 < c < 0.25$ and $0.55 > c > 0.85$.

We next discuss the origin of these regimes for mixtures of ZhK-440 and 5CB in absence of UV irradiation. The pure component ZhK-440 favours tangential anchoring. On increasing amount of polar 5CB dopant, homeotropic anchoring is formed $0.21 \leq c \leq 0.72$. Note that pure 5CB enforces tangential anchoring at various boundaries such as glycerol, polyvinylbutyral or water. Therefore, in general, appropriate surfactants are needed to enable homeotropic anchoring. As reported previously, *bipolar–radial* structural transformation can be triggered by 3.5% of lipid lecithin dispersed in polymer/LC [38], by 1 mM concentration of synthetic lipid sodium dodecyl sulfate (SDS) [3] or by pg/ml concentration of bacterial glycolipid Lipid A in water [17,25]. In particular, it has been reported that *radial* configuration was formed in the time, less than 1 min after the injection of lipids into LC emulsion [3]. In our case, observation of the *radial* configuration within the droplets was found outright after immersing of microscope objective into the LC emulsion which required a few seconds. Moreover, we used large number of LC droplets and the presence of contaminants is restricted by usage of apyrogenic materials, thus, spontaneous formation of radial *droplets* was not due to presence of impurities. The majority of our mixtures contained photosensitive molecules with possibility of *trans-cis* configurational transformation. For this reason negative light-induced *bipolar*-to-*radial* structural transition [26] was protected by usage of green filter, placed between light source and polariser. Cyanobiphenyls are polar molecules and mixtures with non-polar mesogens such as azoxy compounds usually produce induced/enhanced smectic-A mesophase often due to complex formation [39]. For example, Kurik et al. observed radial configuration with a uniform interference pattern and cross like extinction bands which was assigned to formation of smectic-A layers of n-nonyloxy-benzoic acid butoxphenyl ester oriented tangentially at the boundary of glycerol matrix doped by lecithin [40]. Murazawa et al. reported the existence of radial configuration exhibited the same optical texture for 4′-octyl-4-biphenylcarbonitrile (8CB) SmA droplets confined by heavy water D_2O without any surfactants [41]. Thereby, enhanced SmA phase in the mixture ZhK-440/5CB (where $0.4 \leq c \leq 0.55$) can form *radial* director configuration within the droplets with optical pattern similar to nematic mesophase. For this reason, we studied thin layers of the mixtures ($0.25 \leq c \leq 0.58$), confined to 18-μm glass cell treated by rubbed polymer to provide planar/twist structure. Polarised optical microscopy observations showed uniformly aligned planar/twist structure of typical nematic phase at least from $T \sim 21^{\circ}$C to LC–isotropic phase transition. Moreover, our mixtures possessed low viscosity, whereas *Sm*A phase is highly viscous material. Oppositely to 5CB, ZhK-440 has a wide temperature of nematic phase, therefore temperature range of mesophase mixtures decreases with c. So, all mixtures were studied at random temperature, respectively, to the nematic–isotropic phase transition. Nevertheless, no changes in interference patterns were observed for $0.4 \leq c \leq 0.55$ with variation of the temperature, where LC–isotropic phase transition revealed vanishing of the point defect in the centre of the droplet before formation of isotropic phase. We also probed highly polar mixture E7 and non-polar N-(4-Methoxybenzylidene)-4-butylaniline (MBBA) as dopants B and found similar optical textures for E7 and no dopant-induced structural transformations for MBBA.

We next consider changes in the effective elasticity on increasing c. We calculate the effective Frank elastic constants $K_i^{(eff)}$ of mixtures using the approximate expression [1]

$$K_{ii}^{(eff)} = \left((1-c)\sqrt{K_{ii}^{(A)}} + c\sqrt{K_{ii}^{(B)}} \right)^2, \tag{26}$$

where $K_{ii}^{(A)}$ and $K_{ii}^{(B)}$ stand for the Frank elastic constants of the component A and B, respectively. The resulting ratio $K_{33}^{(eff)}/K_{11}^{(eff)}$ is plotted in Figure 5 and monotonously increases with c. Note that the classical radial structure depends only on the splay elastic constant K_{11}. On the other hand, in bipolar structures, the nematic bend elastic constant weighted by K_{33} also plays important role. Therefore, the increasing ratio $K_{33}^{(eff)}/K_{11}^{(eff)}$ is in favour of radial structures. Furthermore, flexoelectricity [42] is expected to play important role in LC droplets in the

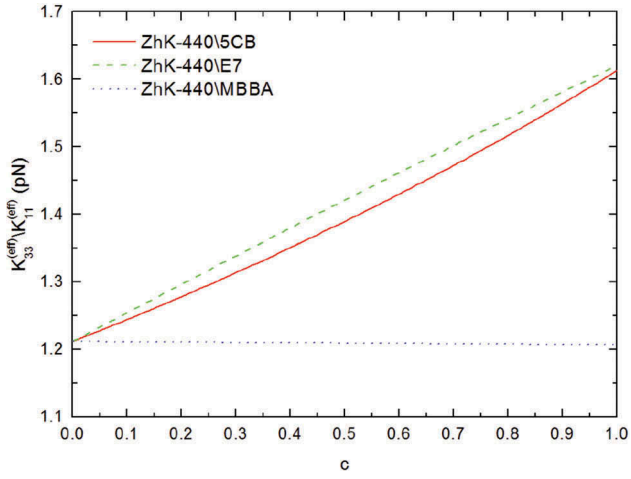

Figure 5. (Colour online) The ratio of effective Frank elastic constants $K_{33}^{(eff)}/K_{11}^{(eff)}$ as a function of concentration c of dopant B. As B we consider either 5CB, E7 or MBBA nematic phase.

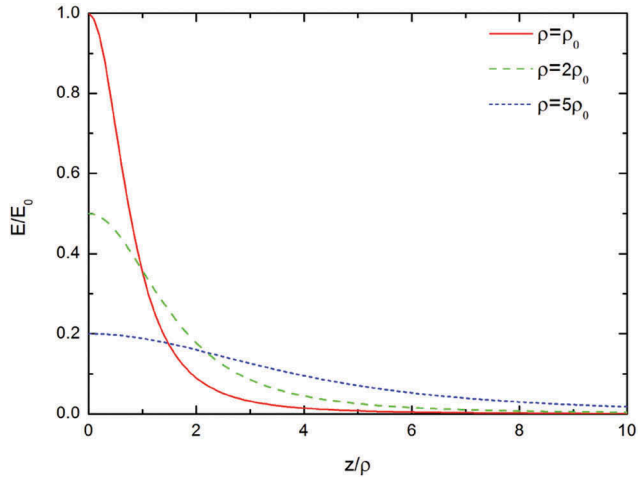

Figure 6. (Colour online) The electric field as a function of distance z above homogeneously distributed electric dipoles within a cylindrical layer of radius ρ (see Equation 6). Solid line: $\rho = \rho_0$, dashed line: $\rho = 2\rho_0$, dotted line: $\rho = 5\rho_0$; $E_0 = \sigma/(2\varepsilon_0\rho_0)$, σ is surface density of dipoles and $\rho_0 = 1$ nm.

micrometre regime. If an effective radially oriented electric field is present, it is expected to promote *radial* structures. Therefore, elasticity alone could explain stabilisation of *radial* structures in the window $0 \leq c \leq 0.55$. However, *bipolar* structures are reentered for $c > 0.55$. Therefore, elasticity could not yield explanation for the observed features, at least for relatively high concentrations c.

We claim that electrostatic interactions are responsible for the observed phenomenon. In Section 3.1, we calculated dipole interaction between a LC molecule carrying an electric dipole and the image dipole in dielectric water medium, where details are given in [29]. In case of *trans*-isomers, where the dipole is roughly aligned along the local director fields, the interaction favours homeotropic anchoring at the LC–water interface as suggested in Equation 3. However, due to steric interactions, tangential anchoring is realised [29]. Added polar component B could enforce homeotropic anchoring. Namely, in Section 3.2, we showed that appropriate assemblies of electric dipoles could yield relatively large electric fields at interfaces hosting the dipoles [30]. In Figure 6, we plot an electric field above an interface hosting homogeneously distributed electric dipoles within a cylindrical layer of radius ρ (see Figure 1). One sees that for nanoparticle-type assemblies, where ρ is of order nanometre, one gets relatively strong and localised electric field above the interface. With increasing ρ, the field magnitude decreases and also decaying of the field strength on increasing the distance from the interface becomes progressively flatter. Therefore, one possibility is that for intermediate concentrations c (i.e. within the concentration window $0.22 \leq c \leq 0.72$), assemblies of 5CB molecules act as nanoparticle-like objects carrying electric dipoles. Note that within the droplet, 5CB molecules exhibit head-to-tail invariance. However, at the surface, collective effect of the assembled 5CB molecules coupled with electric dipoles of water enclosing the LC droplets could break this invariance. In Section 3.3, we showed that water permittivity could be strongly influenced by an electric field. The resulting effective electrostatic coupling could be strong enough to support homeotropic anchoring. For higher concentration of 5CB molecules, their dipoles lose their nanoparticle character because they effectively form assemblies characterised by radius ρ, for which the resulting electric field is relatively weaker (see Figure 6). Consequently, their coupling with surrounding water dipoles is weaker and steric interactions promoting tangential anchoring prevail.

Figure 7 shows the dependence of water permittivity ε_w on the normalised value of electric field strength. It can be seen that ε_w is decreasing with the increasing magnitude of electric field strength E due to saturation effect in water dipole orientational ordering.

4.2. Influence of c in the presence of UV light irradiation

The UV irradiation of intensity I triggers the *bipolar–radial* transition (Figure 8) for reasonable irradiation times (not exceeding 30 min) only in the concentration window $0.08 \leq c \leq 0.2$.

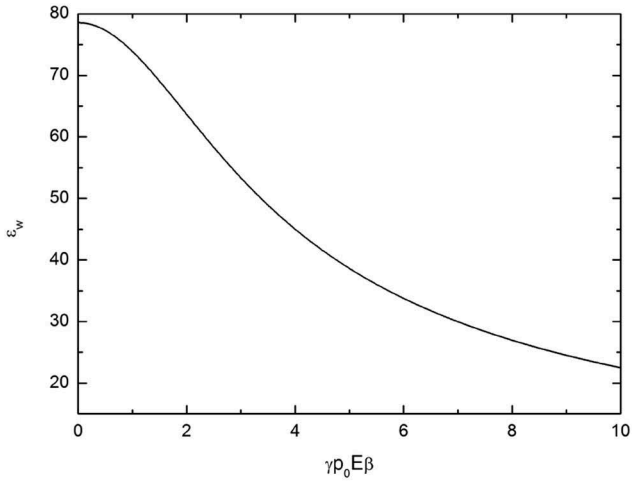

Figure 7. The dependence of water permittivity ε_w on the electric field strength calculated by using Equation 14 at room temperature. The values of the model parameters are $p_0 = 3.1D$ and $n_w/N_A = 55$ mol/l [43].

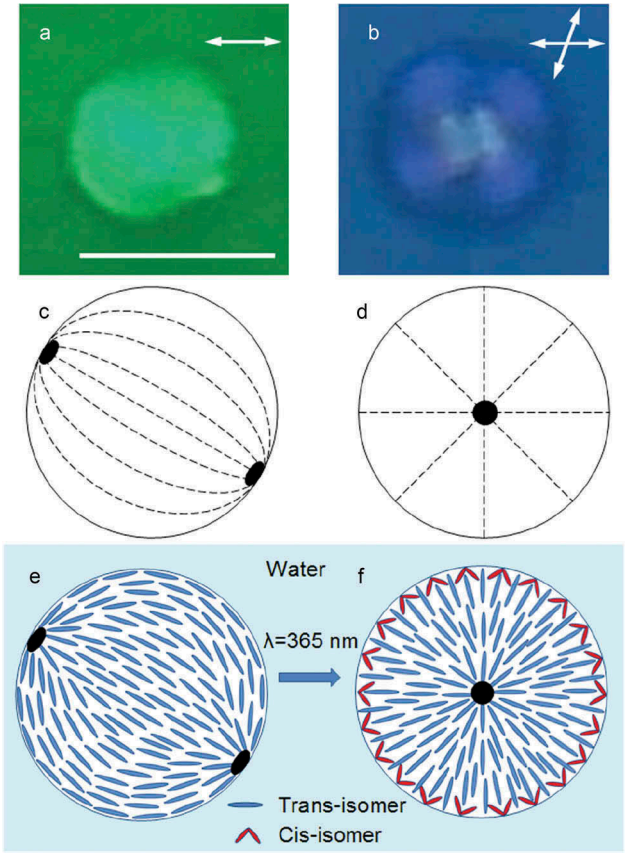

Figure 8. (Colour online) POM images (A, B) of LC droplet, sketches of director configuration (C, D) and schematic distribution of *trans-cis* isomers (E, F) within the LC droplet in water before (A, C, E) and after (B, D, F) UV irradiation (10 s of exposure, $c = 0.16$, $I = 40$ mW/m^2). Double-headed arrows indicate the orientation of the single polariser (A) and the crossed polarisers (B). Scale bar is 5 μm.

We next consider an impact of UV irradiation on *bipolar–radial* structural transitions in the regime $0.08 \leq c \leq 0.2$. In Figure 9, we plot the critical irradiation time t_c as a function of R and c. The critical time monotonously increases with R exhibiting roughly linear dependence on R.

Dependence of t_c as a function of the UV irradiation intensity is emphasised in Figure 10.

Behaviour of t_c on varying R and I is well explain using a simple model presented in Section 3.4. The UV radiation causes the transition due to the assembling of *cis*-isomers at the interface [26]. They promote homeotropic anchoring mainly due to steric reasons [44]. When the ratio between *cis*-isomers and *trans*-isomers reaches a critical value, the structural transition takes place. To explain qualitatively the observed $t_c(R)$ dependence, it is necessary to assume that the UV absorption is efficient only in a narrow frontal lobe within a finite penetration thickness. For example, if the whole droplet volume is irradiated, then $t_c(R)$ dependence would relatively weakly depend on R. It would even decrease with increasing R because *cis*-isomers have stronger preference to assemble at the LC–water interface in comparison with *trans*-isomers [44] (see Equation 3).

Decreasing of t_c on increasing c of polar dopant (see Figures 9 and 10) can be also explained by considering electrostatic interactions. Note that in rod-like polar dopant of our interest, their dipole orientation roughly coincides with their characteristic long axis orientation. Our explanation is as follows. When *cis*-isomers assemble at the LC–water interface, they align their electric

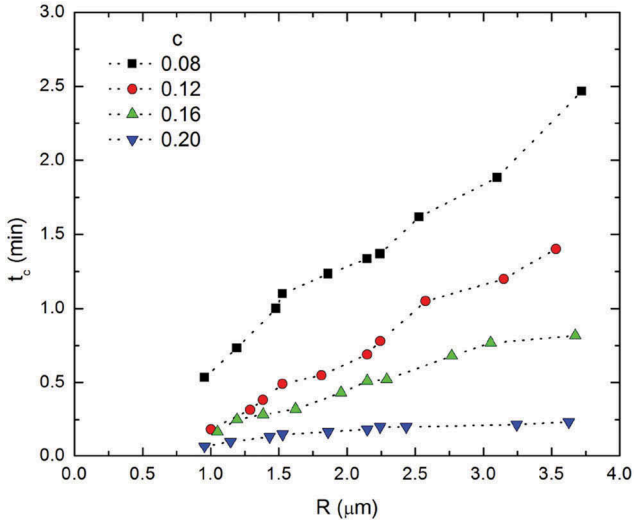

Figure 9. (Colour online) Dependence of the critical irradiation time t_c on the droplet radius R for different concentration c of the polar 5CB dopant. $I = 40$ mW/m^2.

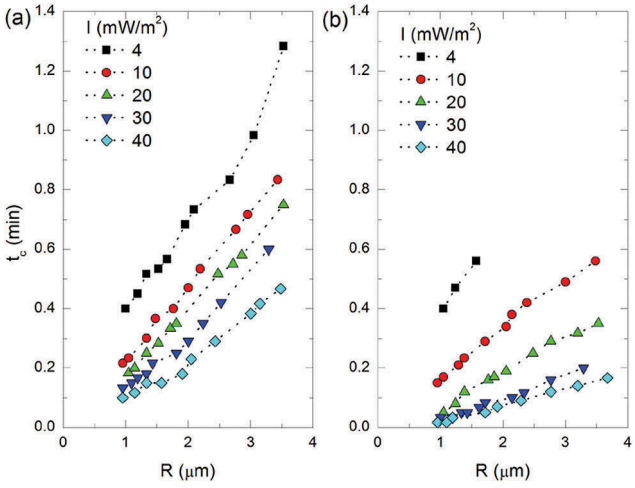

Figure 10. (Colour online) Variation of t_c on changing R and intensity I of UV irradiation for dopant 5CB: (a) $c = 0.12$, (b) $c = 0.16$.

dipoles along the interface normal due to steric effects [29,44]. They consequently induce dipoles in the enclosing water interface layer (see Section 3.3). This in turn tends to align polar dopants homeotropically at the interface due to the electrostatic coupling. Consequently, if concentration of dopants is not too high (see Equation 6) the effective interaction between interface assembled LC dipoles and surrounding water interface layer promotes homeotropic anchoring. Consequently, the critical irradiation time t_c needed to trigger the structural transition decreases with increasing c.

In addition to 5CB dopant, we probed also E7 LC. Both dopants are polar. For cases studied, they exhibit qualitatively similar t_c variation on varying R as it is demonstrated in Figure 11.

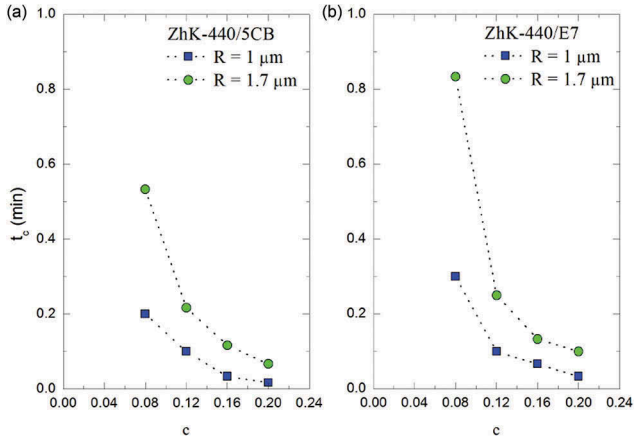

Figure 11. (Colour online) Variation of t_c on varying c of polar dopant: (a) 5CB, (b) E7. Light intensity $I = 40$ mW/m^2.

Since lower concentration of *cis*-isomers is needed to induce the *radial* configuration at increasing of c, it is expected that the sensitivity of orientational structure to impurities can be increased by moving the system close to the bipolar–radial transition with appropriate choice of polar dopant concentration. Such investigations are in progress now and will be presented elsewhere.

5. Conclusion

We studied the influence of polar dopant on internal director configuration of azoxybenzene nematic-in-water droplets. We found a sequence of *bipolar-radial-bipolar* director transformations with increasing of concentration of the polar dopant. Both pure azoxybenzene ZhK-440 and cyanobiphenyl 5CB were tangentially oriented on LC-water boundary whereas their mixtures formed homeotropic anchoring. On increasing c we established three different regimes in the absence of UV irradiation where LC droplets exhibited *bipolar* configuration (intermediate structures) in the ranges $0 \leq c \leq 0.2$ and $0.85 \leq c \leq 1$ ($0.2 < c < 0.25$ and $0.58 > c > 0.85$). Within the concentration window $0.25 \leq c \leq 0.58$ the droplets spontaneously form *radial* structures. We also triggered the *bipolar–radial* structural transition by UV light irradiation of emulsion, involving *trans-cis* isomerisation of nematic molecules. The critical irradiation time needed for *radial* configuration formation was found to decrease with polar dopant's concentration. For concentration range $0.08 \leq c \leq 0.2$, we established decreasing of critical irradiation time from minutes to seconds which is important for biosensing applications. Our theoretical description is based on simple phenomenological model taking into account electrostatic interactions responsible for observed phenomena. The proposed model qualitatively explains our main experimental results.

Acknowledgement

A.I. gratefully acknowledges the help of Ekaterina Gongadze. A.V.D. acknowledges V.S. Bezborodov for useful discussion.

Disclosure statement

No potential conflict of interest was reported by the authors.

Funding

This work was partially supported by the Ministry of Education and Science of the Russian Federation [Grant No. 3.1921.2014/K and Grant of the President of Russia for young scientists No. MK-4886.2016.2] and by the Russian

Foundation for Basic Research [Grant No. 15-32-21143]. S.K. acknowledges the financial support from the Slovenian Research Agency [research core funding Nos. P1-0099 and P2-0232].

ORCID

A. V. Dubtsov http://orcid.org/0000-0001-9999-0347
S. V. Pasechnik http://orcid.org/0000-0002-6050-2761
D. V. Shmeliova http://orcid.org/0000-0003-3869-8806
D. A. Semerenko http://orcid.org/0000-0002-7050-2677
Aleš Iglič http://orcid.org/0000-0002-7895-343X
Samo Kralj http://orcid.org/0000-0002-3962-8845

References

[1] Pasechnik S, Chigrinov V, Shmeliova D. Liquid crystals: viscous and elastic properties in theory and applications. Weinheim: Wiley; 2009.
[2] Brake JM, Daschner MK, Luk YY, et al. Biomolecular interactions at phospholipid-decorated surfaces of liquid crystals. Science. 2003;302(5653):2094–2097.
[3] Gupta JK, Zimmerman JS, De Pablo JJ, et al. Characterization of adsorbate-induced ordering transitions of liquid crystals within monodisperse droplets. Langmuir. 2009;25:9016–9024.
[4] Drzaic P. Liquid crystal dispersions. world scientific. Singapore: River Edge; 1995.
[5] Crawford G, Žumer S. Liquid crystals in complex geometries: formed by polymer and porous networks. London: CRC Press; 1995.
[6] Polak RD, Crawford GP, Kostival BC, et al. Optical determination of the saddle-splay elastic constant *k*24 in nematic liquid crystals. Phys Rev E. 1994;49:R978.
[7] Doane JW, Vaz NA, Wu BG, et al. Field controlled light scattering from nematic microdroplets. Appl Phys Lett. 1986;48(4):269–271.
[8] Bondar VG, Lavrentovich OD, Pergamenshchik VM. Threshold of structural hedgehog-ring transition in drops of a nematic in an alternating electric field. Zh Eksp Teor Fiz. 1992;101:111–125.
[9] Candau S, Roy PL, Debeauvais F. Magnetic field effects in nematic and cholesteric droplets suspended in a isotropic liquid. Mol Cryst Liq Cryst. 1973;23(3–4):283–297.
[10] Koval'chuk AV, Kurik MV, Lavrentovich OD, et al. Structural transformations in nematic droplets located in an external magnetic field. Zh Eksp Teor Fiz. 1988;94:350–364.
[11] Mushenheim PC, Abbott NL. Hierarchical organization in liquid crystal-in-liquid crystal emulsions. Soft Matter. 2014;10(43):8627–8634.
[12] Golemme A, Žumer S, Allender DW, et al. Continuous nematic-isotropic transition in submicron-size liquid-crystal droplets. Phys Rev Lett. 1988;61:2937–2940.
[13] Erdmann JH, Žumer S, Doane JW. Configuration transition in a nematic liquid crystal confined to a small spherical cavity. Phys Rev Lett. 1990;64:1907–1910.
[14] Fernández-Nieves A, Link DR, Márquez M, et al. Topological changes in bipolar nematic droplets under flow. Phys Rev Lett. 2007;98:087801.
[15] Carlton RJ, Hunter JT, Miller DS, et al. Chemical and biological sensing using liquid crystals. Liq Cryst Rev. 2013;1(1):29–51.
[16] Miller DS, Wang X, Abbott NL. Design of functional materials based on liquid crystalline droplets. Chem Mater. 2014;26(1):496–506.
[17] Lin IH, Miller DS, Bertics PJ, et al. Endotoxin-induced structural transformations in liquid crystalline droplets. Science. 2011;332:1297–1300.
[18] Dubtsov AV, Pasechnik SV, Shmeliova DV, et al. Controlled nanoparticle targeting and nanoparticle-driven nematic structural transition. Adv Cond Matter Phys. 2015;2015:803480.
[19] Sivakumar S, Wark KL, Gupta JK, et al. Liquid crystal emulsions as the basis of biological sensors for the optical detection of bacteria and viruses. Adv Funct Mater. 2009;19:2260–2265.
[20] Chen CH, Yang KL. A liquid crystal biosensor for detecting organophosphates through the localized ph changes induced by their hydrolytic products. Sens Actuat B Chem. 2013;181:368–374.
[21] Luk YY, Tingey ML, Dickson KA, et al. Imaging the binding ability of proteins immobilized on surfaces with different orientations by using liquid crystals. J Am Chem Soc. 2004;126:9024–9032.
[22] Kim J, Khan M, Park SY. Glucose sensor using liquid-crystal droplets made by microfluidics. ACS Appl Mater Interfaces. 2013;5(24):13135–13139.
[23] Wang X, Kim YK, Bukusoglu E, et al. Experimental insights into the nanostructure of the cores of topological defects in liquid crystals. Phys Rev Lett. 2016;116:147801.
[24] Wang X, Miller DS, Bukusoglu E, et al. Topological defects in liquid crystals as templates for molecular self-assembly. Nat Mat. 2016;15:106–112.
[25] Carter MCD, Miller DS, Jennings J, et al. Synthetic mimics of bacterial lipid a trigger optical transitions in liquid crystal microdroplets at ultralow picogram-per-milliliter concentrations. Langmuir. 2015;31(47):12850–12855.
[26] Dubtsov AV, Pasechnik SV, Shmeliova DV, et al. Light and phospholipid driven structural transitions in nematic microdroplets. Appl Phys Lett. 2014;105:151606.
[27] Barnik MI, Belyaev SV, Grebenkin MF, et al. Electrical, optical and viscoelastic properties of liquid-crystal mixture of azoxycompounds. Sov Crystallogr. 1978;23:451.
[28] Aronzon D, Levy EP, Collings PJ, et al. Transcis isomerization of an azoxybenzene liquid crystal. Liq Cryst. 2007;34:707–718.
[29] Barbero G, Evangelista LR, Komitov L. Photomanipulation of the anchoring strength of a photochromic nematic liquid crystal. Phys Rev E. 2002;65:041719.
[30] Chkhartishvili L. Nanoparticle near-surface electric field. Nanoscale Res Lett. 2016;11(1):48.
[31] Gongadze E, Iglič A. Decrease of permittivity of an electrolyte solution near a charged surface due to saturation and excluded volume effects. Bioelectrochemistry. 2012;87:199–203.

[32] Gongadze E, Velikonja A, Perutkova S, et al. Ions and water molecules in an electrolyte solution in contact with charged and dipolar surfaces. Electrochimica Acta. 2014;126:42–60.
[33] Fröhlich H. Theory of dielectrics. Oxford: Clarendon Press; 1964.
[34] Blinov L, Chigrinov V. Electrooptic effects in liquid crystal materials. New York: Springer-Verlag; 1994.
[35] Chen H, Zhu R, Zhu J, et al. A simple method to measure the twist elastic constant of a nematic liquid crystal. Liq Cryst. 2015;42(12):1738–1742.
[36] Stewart I. The static and dynamic continuum theory of liquid crystals. London: Taylor and Francis; 2004.
[37] Miller DS, Abbott NL. Influence of droplet size, ph and ionic strength on endotoxin-triggered ordering transitions in liquid crystalline droplets. Soft Matter. 2013;9:374–382.
[38] Prischepa OO, Shabanov AV, Zyryanov VY. Director configurations within nematic droplets doped by lecithin. Liq Cryst. 2005;438:141 [1705]–150 [1714].
[39] Kumar S. Liquid crystals: experimental study of physical properties and phase transitions. Cambridge: Cambridge University Press; 2000.
[40] Kurik MV, Lavrentovich OD. Monopole structures and shape of drops of smectics-c. Sov Phys JETP. 1983;58:299–307.
[41] Murazawa N, Juodkazisa S, Misawa H. Laser manipulation of a smectic liquid-crystal droplet. Eur Phys J E. 2006;20:435–439.
[42] Lavrentovich OD. Flexoelectricity of droplets of a nematic liquid crystal. Sov Tech Phys Lett. 1988;13:166–171.
[43] Gongadze E, Velikonja A, Slivnik T, et al. The quadrupole moment of water molecules and the permittivity of water near a charged surface. Electrochimica Acta. 2013;109:656–662.
[44] Barbero G, Popa-Nita V. Model for the planar-homeotropic anchoring transition induced by trans-cis isomerization. Phys Rev E. 2000;61:6696–6698.